User Guide to

the EDI measurements

in the Cluster Active Archive (CAA)

prepared by

E. Georgescu and the EDI team

maintained by

M. Rashev

Reference Documents

[1] EDI CAA Interface Control Document. ()

[2] Paschmann G. et al., The Electron Drift Instrument on Cluster: overview of first results, Annales Geophysicae (2001) 19: 1273–1288. (https://caa.esac.esa.int/caa/instr_doc.xml)

[3] Quinn, J. M., Cluster EDI convection measurements across the high-latitude plasma sheet boundary at midnight, Annales Geophysicae (2001) 19: 1669–1681. (https://caa.esac.esa.int/caa/instr_doc.xml)

[4] Georgescu E. et al., EDI data products in the Cluster Active Archive, in *The Cluster Active Archive - Studying the Earth's Space Plasma Environment*, edited by H. Laakso, M. Taylor and C. P. Escoubet, pp. 83-96, Springer, 2010.

[5] Users Guide to the Cluster Science Data System, DS–MPA–TN–0015, issue3, 2008, (https://caa.esac.esa.int/documents/publications/csds_guide_3_0.pdf)

[6] Georgescu et al, Cross Calibration Report of the EDI Measurements in the Cluster Active Archive (CAA), CAA-EST-CR-EDI. (https://caa.esac.esa.int/caa/ug_cr_icd.xml)

[7] Paschmann G. et al, The Electron Drift Instrument for Cluster. Space Science Reviews (1997), 79, 233–269

[8] CAA Command Line Download Document, (https://caa.esac.esa.int/documents/CAA-EST-CMDLINE-0015.pdf)

[9] Förster, M., G. Paschmann, S. E. Haaland, J. M. Quinn, R. B. Torbert, C. E. McIlwain, H. Vaith, P. A. Puhl-Quinn, and C. A. Kletzing (2007), High-latitude plasma convection from Cluster EDI: Variances and solar wind correlations, Ann. Geophys., 25, 1691–1707.

[10] Haaland, S., et al. "Plasma convection in the magnetotail lobes: statistical results from Cluster EDI measurements." Annales Geophysicae. Vol. 26. No. 8. Copernicus GmbH, 2008.

Acronyms

AE	Ambient Electron
CR	Calibration Report
EDI	Electron Drift Instrument
GDU	Gun Detector Unit
ICD	Interface Control Document
MCP	Multichannel Plate Detector
TOF	Time-of-flight
TRI	Triangulation
WW	Windshield Wiper instrument operation mode

Table of Content

1 Introduction

The Electron Drift Instrument (EDI) measures, depending on its operation mode, either the electron drift (and electric field) or ambient electron counts:

- EDI complements the measurements by double-probe technique (EFW instrument) in that the EDI measurements are essentially unaffected by the spacecraft environment and include the component of the electric field along the spacecraft spin axis.

- The EDI ambient electron counts are high time resolution (of the order of milliseconds), but for a fixed narrow energy and pitch angle and are uncalibrated. Ambient electron fluxes for similar energies and pitch angles are measured by PEACE (at about 0.5 sec resolution during burst mode, and at spin resolution at other times).

This User Guide presents shortly the EDI instrument, its operation modes and its key data products in the CAA; all EDI datasets are listed in appendix A.

2 Instrument Description

The essential elements of the instrument are two electron guns, two detectors with their associated analogue electronics, high-voltage supplies, digital controls, and correlators, and a controller unit that includes the interfaces with the spacecraft and with other instruments.

Guns and detectors are combined in pairs into a single unit, referred to as the gun/detector unit (GDU), see Figure 1. Two GDUs are mounted on each spacecraft separated by 180°, each detector measuring the electrons emitted by the gun placed opposite to it. The electron beams are swept rapidly back and forth around the direction perpendicular to the magnetic field in a windshield-wiper type of motion in order to reach the detectors. The beam direction and the time-of flight of the electrons are recorded for every successful detection. The emitted electrons are either 0.5 or 1 keV; the used energies are given in the Status parameter of the electron drift datasets.

Figure 1 EDI Gun Detector Unit (GDU).
The central part is the electron gun capable of providing narrow beams in any direction within more than a hemisphere, the collar around it divides in 8 sections the entrance grid of the detector. The detector, consisting of an optics section and an annular micro-channel plate (MCP), is able to look in any direction within a region greater than a 2π steradian hemisphere and change the look directions in any direction within two milliseconds (done electronically).

EDI measures the drift of artificially injected electrons in the plane perpendicular to the ambient magnetic field **B;** the measurement principle is explained in Appendix B. The drift is proportional to the component of the electric field $\mathbf{E}_\perp$ in the plane perpendicular to **B**, when the gradient of **B** in this plane can be neglected. Appendix C presents a short assessment of this caveat. In order to know the direction of the local magnetic field, the raw magnetic field information is received through the Inter-Experimental Link (IEL); it is time-tagged and calibrated on board using uploaded calibration matrices.

The success of the electric field measurements is limited by low magnetic fields, rapid time-variations in magnetic and/or electric fields and/or high background electron fluxes.

Whenever the guns are not working, the detectors are used to count the ambient electrons for a fixed energy and pitch angle over a time interval depending on the telemetry mode (see Section 3.2). The EDI instrument and its modes of operation are described in detail in the ICD [1] and the instrument papers by Paschmann et al. [2] and Quinn et al. [3].

3 Instrument Operations

EDI operates in one of two modes:

(1) active mode:　the guns emit electrons. This is also called the **WW** (windshield wiper) mode to illustrate the way the gun is operated, or, the **EF** (electric field) mode to indicate the derived science output of the measurement

(2) passive mode:　the guns do not emit; this is called the ambient electron mode (**AE**).

The time intervals for the operation modes are listed in the Instrument Modes dataset (CLIST), where the acronyms "WW" and "AE" are used for the two operation modes. **The operation mode is the same for both GDUs of an EDI on a spacecraft.**

3.1 Electric field mode

Whenever EDI operates in WW mode, the drift velocity **V** of the electrons can be measured and using $\mathbf{E} = \mathbf{V} \times \mathbf{B}$ the DC electric field is determined. The highest possible time resolution in the WW mode (i.e. transmitted to the ground) is limited to 1/8 s in NM and 1/64 s in BM.

The key operation parameters in WW mode are the energy of the emitted electrons, the code repetition frequency (frequency of emitted electron beam intensity) and the beam intensity (for details, see the ICD). Their values have no relevance for the scientific analysis of the EDI observations. They are contained, however, in the CRF dataset to help the wave instruments to detect interferences caused by EDI. The large beam current is known to drive the spacecraft potential very positive (hundreds of volts) in low plasma density.

In regions of weak magnetic fields high beam currents are required to overcome the beam divergence along large gyro-orbits, and to get sufficient signal-to-background ratio. However, large beam currents, in conjunction with the beam-modulation and –coding, lead to interference with the electric wave measurements by the WHISPER instrument.

Because of these interferences, the EDI beam operations have been subject to restrictions on current intensities over certain orbits. A scheme of the EDI beam operations for Cluster 1, 2, 3 is presented in Figure 2 (note that EDI is not operational on Cluster 4).

Ambient electrons during EF mode

EDI provides an ancillary dataset, called "Background electron counts (in WW mode)" [dataset id - QZC (quality zero counts)] in WW mode that can be used for monitoring background electrons during intervals when the emitted electrons do not return to the detector; for details of this dataset, see Section 5.2.4.
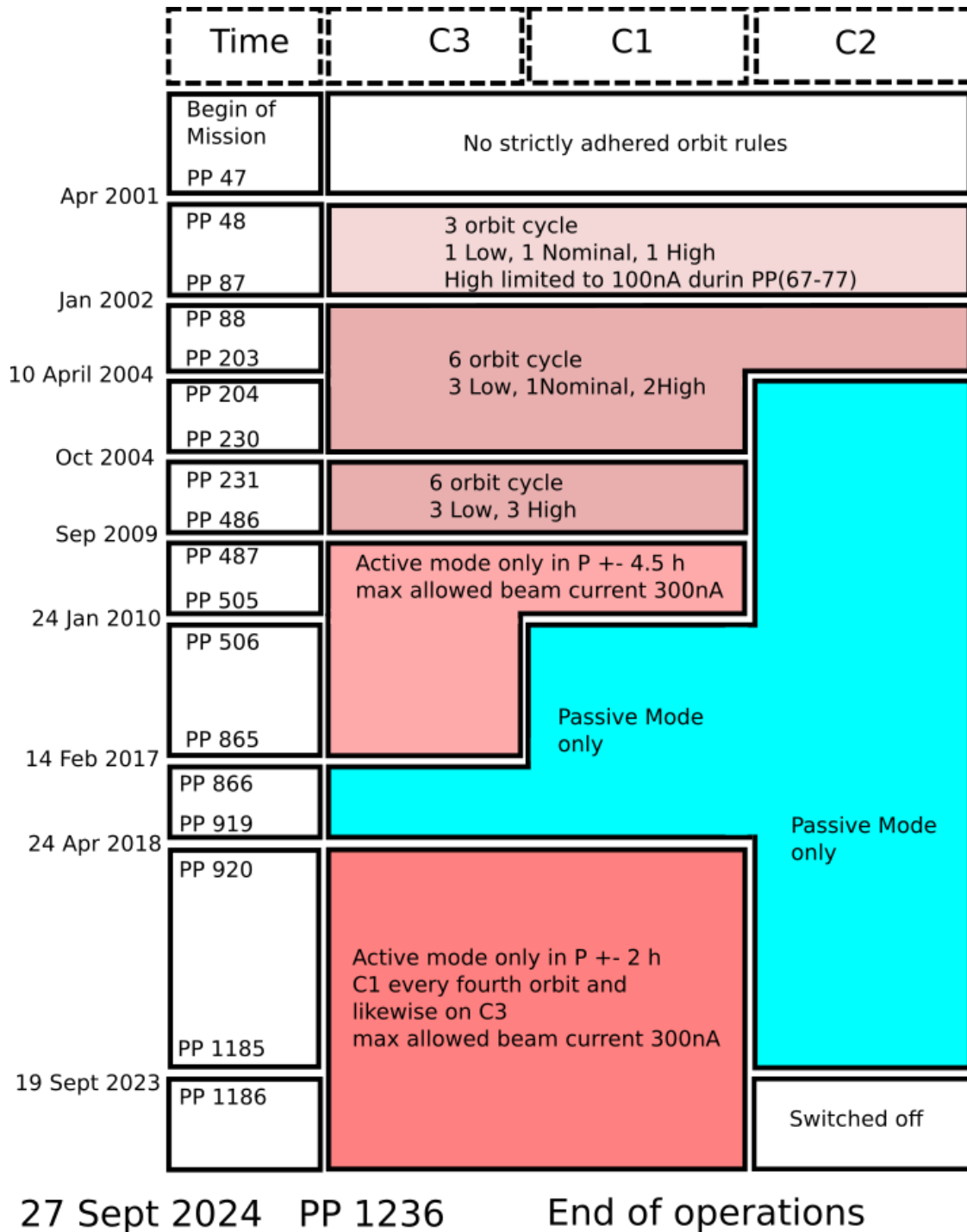
Figure 2 EDI beam operations. PP xxx are the weekly planning periods. The beam current operation modes over an orbit are defined as:

- Low: WW only around perigee P +/-4.5 hrs, where P is the time of perigee, beam current max 45 nA
- Nominal: WW beam current limited to max 45 nA
- High: WW beam current limited to max 300 nA

Exceptions from these definitions are given in the table.

More recently a single operation mode is used: WW (active mode) only around perigee P +/- 4.5 hrs with beam current limited to 300 nA.

However, it is good to notice that injected current is not stable but can vary. On Cluster 2, the beam stability was poor and higher currents than anticipated have been emitted.

There were some active mode tests done in October and December of 2017 for C1 and C3. These tests were done to assess the feasibility of starting to use active mode again on C1 and C3 for the purpose of cross-calibration with other instruments. The dates for these tests are:
October 23/25 2017 (PP 899)
December 18/21 2017 (PP 907).

3.2 Ambient electron mode

The data from Ambient Electron (AE) mode operations are available in the CAA starting 13 October 2004.

In the AE mode, ambient electron counts are recorded at pitch angles of 0º/180º and/or 90º with a high time resolution: 1/16 s in normal (NM) and 1/128 s in burst (BM) telemetry. Notice that the accumulation time intervals for counts are ~16 ms (1/64 s), 25% duty cycle and ~8ms (1/128 s), 100% duty cycle, in NM and BM, respectively. There are two key parameters for the monitoring setup:
- the energy of ambient electrons (0.5 or 1 keV) and
- the pitch angle where the monitored pitch angles can have three alternatives:
  - only 90° or
  - both 0° and 180° degrees, or
  - alternating between 90° and 0°/180° at a selectable frequency which is limited in principle only by the sample accumulation time.

Because of an on-board coding error, the AE data in the early phase of the mission is strongly corrupted until 13 October 2004. Therefore, these data are not archived in the CAA.

From 14 October 2004 until 3 December 2005 a 3 orbit-cycle was used in the "AE"-mode:
      orbit 1:   0.5 keV, fixed at 90º pitch angle
      orbit 2:   0.5 keV, fixed at 0/180º pitch angle
      orbit 3:   1.0 keV, alternating between 0º/180º and 90º pitch angle every ~64 s
Starting 3 December 2005 till now, a 6-orbit cycle is being used:
      orbit 1:   0.5 keV, fixed at 90º pitch angle
      orbits 2, 4, 5:   0.5 keV, fixed at 0/180º pitch angle
      orbit 3 and 6:   0.5 keV, fast alternating between 0º/180º and 90º every ~62.5 ms

3.3 Non-functional instruments

A summary of the gun usage history of EDI is given in Table 1. Once both guns have failed, the instrument can only operate in AE mode. This information is included in the metadata accompanying each data product as INSTRUMENT CAVEATS.

Table 1. Gun Usage History up to the end of 2017

SC	Gun	Last usage in E-Field Mode	Reason	Candidate for future E-field operations
C1	1	Jul 2002	Damage	No
	2	Jan 2010	Interference	Yes
C2	1	Apr 2004	Interference / low success rate	Yes
	2	Apr 2004	Interference	Yes

C3	1	Jul 2010	Interference	Yes (*)
	2	Feb 2017	GDU1 low detector efficiency	No

(*) HK indicates deterioration of Wehnelt Optocoupler, leading possibly to strong emission and a wider than usual electron beam (which would cause stronger interference with WHISPER)

Operations plan since 22 April 2018:
- EDI will be run in E-Field mode every other orbit, alternating between C1 and C3. Every other orbit will be free of EDI E-Field operations. Thus, E-Field mode will be used on C1 every fourth orbit and likewise on C3, with C1 and C3 being out of phase by two orbits.
- E-Field mode will be run over a four-hour interval centered on perigee.

4 Measurement Calibration and Processing Procedures

The WW-mode data are analysed with two techniques: **triangulation (TRI)** and **time-of-flight (TOF)**. A short overview of these techniques with some caveats is given in Appendices B-E and further details can be found in [2], [3], [6] and [7]. The technique which gives better results based on the given error criteria produces the **winners**, the other the **losers**. All results are assigned a **quality** flag (**good / caution / bad**). Information about the used technique and the quality are included in the "Status" parameter of the data records. Only the "PPPlus" dataset (see Appendix A) contains both "winners" and "losers", while the other datasets contain only "winners". This dataset (available for downloading only using "wget" on command line) is meant for expert users while regular users **are not advised** to use it.

If no beam electrons are returned, one may still find records in the Background Electron Counts dataset (see Section 5.2.4).

The electric fields are calculated from the drift velocity measurements using the magnetic field based on the daily calibration files (which are used to produce the CSDS magnetic field prime parameters).

The exact nature and quality of the data is indicated in the seven status bytes described in detail in [5] and the ICD [1] and summarized in Table 2. Regular users need to use only Status(0) while the expert users may also filter data using "Status"-bytes 3, 5, 6.

Table 2. Definition of the Status bytes used in the electric field datasets.

byte	Definition and possible values	Comment
Status(0)	Data quality flag: 0, 1, 2 0= "bad", 1= "use with caution", 2= "good"	The user should filter out "bad" records from the data
Status(1)	% of 1 keV beams per spin 0: only E=0.5 keV is emitted 100: only E=1 keV is emitted, else: energy switching between 0.5 and 1 keV	Can be used for energy filtering (but E=0.5 keV used rarely)
Status(2)	% of high quality beams used in entire spin	Not used for filtering data quality
Status(3)	Method papertrail and Ambiguity flag (bit 7)	See ICD
Status(4)	% of TRI outliers	Not used for filtering data quality
Status(5)	Drift step (S/C frame) magnitude error in %	
Status(6)	Drift step (S/C frame) azimuth error in degrees	

5 Key Science Measurements and Datasets

5.1 Electron drift velocity and DC Electric field

All E-field datasets contain time series of the 3 components of the electron drift velocity and of the 3 components of the electric field **in the inertial Cartesian GSE coordinate system (corrected for spacecraft motion)** with different qualities and time resolution. These variables are called V_ed_xyz_gse__*DatasetID* and E_xyz_gse__*DatasetID,* where *DatasetID* is listed in Appendix A. The SPIN dataset is identical to the PP dataset but without chi_squared variable.

5.1.1 Electron Drift Velocity (GSE), best resolution

This dataset (id = C#_CP_EDI_MP, # = 1, 2, 3) is the highest resolution electric field science product delivered to the CAA by the EDI team and has a variable time-resolution of ~1, ~2 or ~4 seconds. The dataset id of this dataset has a suffix "MP" (Merged Parameter) because these data are obtained by merging the results of processing data with quarter-spin, half-spin, and spin resolution by an algorithm that can be thought as "use more if not lower quality".

Why is the highest resolution a quarter-spin, i.e. 1 s? This is related to the requirement of minimum 7 beams for "GOOD" quality data [1] used by the software. In principle, the maximum resolution in NM mode is 1/8 s which is the period at which the returned electron beam is transmitted to the ground. In BM, this period is 1/64 s (and then one could in principle achieve a temporal resolution of 0.1 s)

This dataset contains measurements of all qualities. The "BAD" data (see Table 2) exists in the MP dataset because it is useful for the advanced user who might be studying data quality itself. It is recommended that the regular CAA user filter out the "BAD" data before using the data for scientific purpose (see Table 2).

5.1.2 Electron Drift Velocity (GSE), spin resolution

This dataset (id = C#_CP_EDI_SPIN, # = 1, 2, 3) is produced from the best resolution dataset by calculating spin averages (~4 sec) using the sun reference pulse. Another important difference between the MP and SPIN datasets is that the poorest quality data (i.e., quality = "BAD" data) have been filtered out of the SPIN dataset.

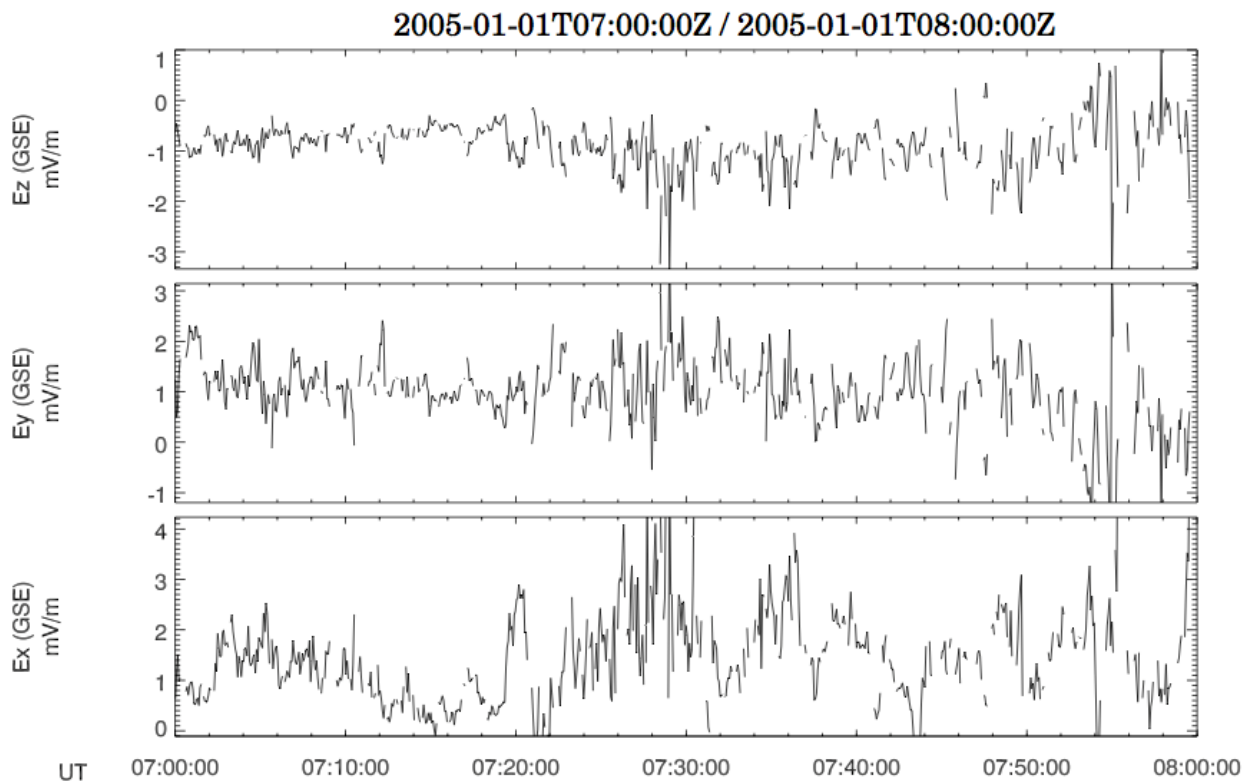Figure 3 shows an example of electric fields data from a SPIN file.

2005-01-01T07:00:00Z / 2005-01-01T08:00:00Z

Figure 3 Plot of the three components of the electric field in GSE from the SPIN dataset using the CSA plotting tool.

5.1.3 Caveats for electric field datasets

The following caveats must be considered:
- the measured electron drift velocity cannot always be separated into the electric-field and magnetic gradient induced parts; in such cases the computed electric fields are subject to contamination by magnetic gradient effects (see Appendix C)
- The data quality is variable, and it is therefore mandatory that the status bytes be consulted before interpreting the data
- The number of samples in the averages is variable
- The measurements are limited by low magnetic fields, rapid time-variations in magnetic and/or electric fields and/or high background electron fluxes
- Presence of multi-runners (see Appendix D)
- Time-aliasing effects (normally unimportant) (see Appendix E)

5.2 Ambient electron measurements

These data consist of time series of ambient raw electron counts for one electron energy, usually 0.5 keV and for one of 3 possible pitch angle combinations (see Section 3.2), the detector look direction in the spacecraft frame and in GSE, and the status for "AE" mode.

Because of an on-board coding error, AE data are not provided before 13 October 2004.

The data in its original form are appropriate only for boundary recognition. One must keep in mind that the EDI detectors are not designed as particle instruments and their detection efficiencies have not been determined prior to the mission and proved to be not constant in time. For science use a transformation to relative particle fluxes can be tried. This transformation involving two corrections and a calibration relative to PEACE is specific to every time interval, because of the variable detector efficiencies and their calibration is not always possible. The procedure is described in [6] and follows the following order:

- The first step is the "**intra-detector**" correction, whereby the angular (theta and phi) dependence are removed from "Ambient electron counts" (id = C#_CP_EDI_AE, # = 1, 2, 3) by using the "Ambient electron correction files" (id = C#_CE_EDI_AEC_TXT, # = 1, 2, 3). The "Corrected ambient electron data" (id = C#_CP_EDI_AEDC, # = 1, 2, 3) dataset includes this correction. All these datasets are available in the CAA.
- The second step is an "**inter-detector**" correction, where the efficiencies of the two detectors are brought to the same level.
- The relative **calibration to PEACE** requires the existence of PEACE differential energy flux data for the time interval of interest.

The users of AE data must do the last two steps by themselves.
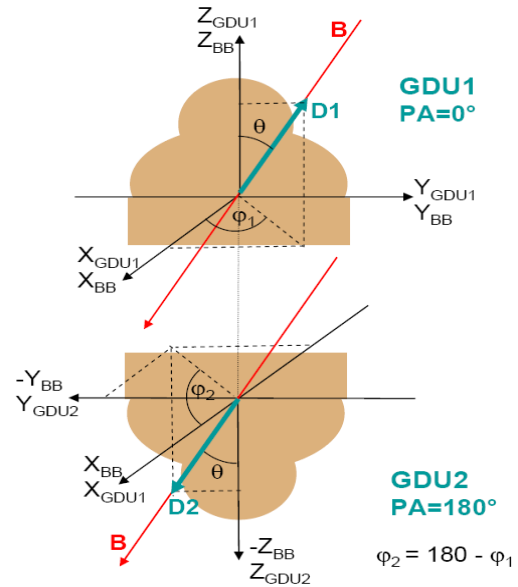
5.2.1 Ambient electron counts

This dataset (id = C#_CP_EDI_AE, # = 1, 2, 3) contains 6 raw data "counts", that is, counts at 0º, 180º and 90º pitch angles from both GDUs. Depending on the orbit, two perpendicular "counts" (90º), four parallel/anti-parallel counts (0º and 180º) or all six counts (0º, 180º and 90º) may contain measurement values; the rest contain fill-values. The count variables are called counts_GDU1_PA_0__*id*, counts_GDU2_PA_0__*id*, counts_GDU1_PA_90__*id*, counts_GDU2_PA_90__*id*, counts_GDU1_PA_180__*id*, counts_GDU2_PA_180__*id.* The supporting variables are:

- STATUS: Only 2 bits of the byte are used:
  - Bit 0 indicates the energy: 1 is used for 1 keV, and 0 is used for 0.5 keV.
  - Bit 1 indicates the telemetry mode: if it is set, the data is from BM1 data; otherwise, the data is from NM1/2/3 or BM2.
- D1_xyz_gse: detector 1 look-direction in Cartesian GSE coordinates.
- Theta_index, Phi_index: look directions of both detectors in spherical instrument frame. The instrument frame for GDU1 is identical with the spacecraft "body-build" frame having the X-axis along the nominal spin-axis and the Z-axis directed radially outward. The GDU2 frame is rotated with 180° around the spin-axis. The EDI instrument frame is sketched in Fig. 4
  - The theta variable is the same for both EDI detectors and contains an index between 0 and 138; each step corresponds to 0.703125 degrees.
  - The phi variable contains an index between 0 and 127 and each step corresponds to 2.8125 degrees. The reported phi is the azimuth look direction for detector 1.
  - The phi for detector 2 is opposite, i.e. phi2 = 64 - phi1, and then adjusted so that it is between 0 and 127 if necessary.

Figure 4. EDI instrument frame. The GDU1 instrument frame has the same coordinate axes as the spacecraft BB (Body-Built): X_{BB} = along the nominal spin axis; Z_{BB} = in spin plane and is radially outward and is symmetry axis for GDU1.

GDU2 frame is rotated with 180° around the spin axis: $Z_{GDU2} = -Z_{BB}$ and $Y_{GDU2} = -Y_{BB}$;

The unit vector of the detector look direction for GDU1 in spherical coordinates is characterized by the polar angle θ and azimuth angle φ.

$\theta = \mathrm{acos}(Z_{BB})$

$\varphi = \mathrm{atan}(Y_{BB}/X_{BB})$

In "AE"-mode: θ has the same value for both GDUs and φ are supplementary: $\varphi 2 = 180 - \varphi 1$. See Figure 1 for the image of the instrument.

5.2.2 Corrected ambient electron counts

This dataset (id = C#_CP_EDI_AEDC, # = 1, 2, 3) is the result of the intra-detector calibration, as explained above. It contains the corrected raw counts, the status, and the GSE direction for D1. An example of these data for a magnetosheath interval is given in Figure 5. We plotted the full resolution data in the bottom two panels and 5 sec averages in the top panel. This is the same averaging interval used in the summary plots that are available for viewing and downloading in the CAA and that show the (uncorrected) raw electron counts data.

Figure 6 shows a summary plot for the interval of Figure 5. Panel 3 from the top shows the raw electron counts. The boundary crossings are visible, so for boundary crossing survey one could easily use the quick-look plots. Only if a more precise determination of the crossing is necessary then it is useful to use the full resolution AEDC data.

5.2.3 Caveats for AE datasets

The following caveats must be considered for the ambient electron data:

- Ambient raw-data counts from the AE dataset have to be corrected for the angular dependence of the efficiency (this is already done for the AEDC dataset) and for the difference in the overall efficiencies of the two detectors. A comparison with PEACE electron fluxes for the same energy and pitch angle is required to determine the calibration factor. For more detail, see [6].
- Ambient electron data are available since Oct 2004 on C1, C2 and C3, the time intervals are listed in Instrument modes dataset (id = C#_CQ_EDI_CLIST, # = 1, 2, 3). The EDI instrument on C2 is working only in ambient mode since April 2004 and on C1 since January 2010.
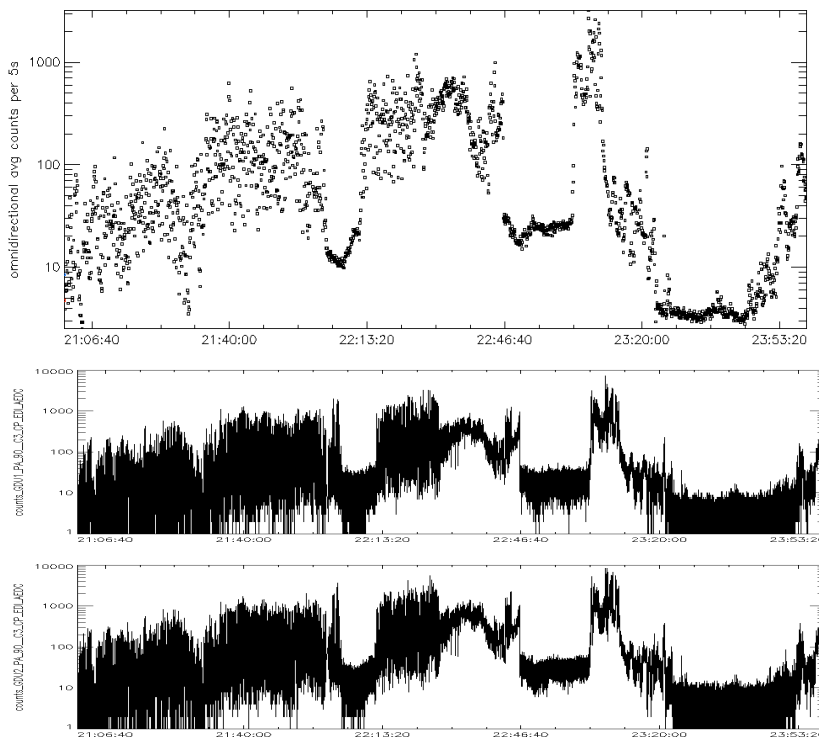
Figure 5 Three hours of **Corrected ambient electron counts (AEDC)** data for Cluster 3, 2005-01-01 EDI instrument frame. Pitch angle is 90°; the full resolution data are shown in the bottom two panels, and 5 s averages in the top panel to ease the comparison with the quick-look plot from Fig.6

5.2.4 Background electron counts

This dataset (id = C#_CQ_EDI_QZC, # = 1, 2, 3) contains time series of the ambient electron counts at 90° pitch angle and fixed energy 1 keV, rarely 0.5 keV, collected during electric field mode. The measured counts are transmitted to the ground at a period of 1/8 s in NM and 1/64 s in BM.

In contrast to the "AE" mode where the two GDU's look exactly in the opposite direction, in the "WW" operation mode the two detectors look in two independent directions determined by the shooting direction of the guns. Both look directions are recorded.

The "counts" variables are called: counts_GDU1_PA_90_*id* and counts_GDU2_PA_90_*id*. The supporting variables are:

- STATUS: Only 2 bits of the byte are used:
    - Bit 0 indicates the sampling mode: 1 means 4 times 1 ms samples and 0 means 2 times 2 ms samples in an operation cycle of 4ms. Note that to get the count rate (in electrons/second) the user has to multiply the electron counts with 1024 if bit0 is set, otherwise with 512.
    - Bit 1 indicates the energy: 0 is used for 1 keV, and 1 is used for 0.5 keV.

- D1_rlp_gse__id: detector 1 look-direction in Spherical GSE coordinates in degrees.

- D2_rlp_gse__id: detector 2 look-direction in Spherical GSE coordinates in degrees.

These raw electron counts may be contaminated by artificial emitted beam electrons.

5.3 Supporting datasets

5.3.1 Instrument modes

This dataset (id=Ci_CQ_EDI_CLIST, i=1, 2, 3) gives an overview of the EDI operation modes; it contains time intervals for ambient electron (AE) and electric field (WW) modes. The time intervals of the two operations modes are also shown in the quick-look plots. (See panel 2 from top in Figure 6).

Being in electric field mode does not mean automatically that the instrument measured successfully the returning electrons and that the data products for the specified mode are present.

5.3.2 Quality Statistics

The daily "Quality Statistics for Electron Drift Velocity measurements" dataset (id=Ci_CE_EDI_QSTAT_TXT, i=1, 2, 3) provides this information by giving the percentage of detected electron beams for every 10 minutes of the day. For the details of this product, see ICD.

5.3.3 Quick-look plots

The EDI quick-look plots (id: CL_CG_EDI_SUMMPLOT) can either be viewed through the CSA quick-look tool at **http://www.cosmos.esa.int/web/csa/csds-quicklook-plots** or be downloaded.
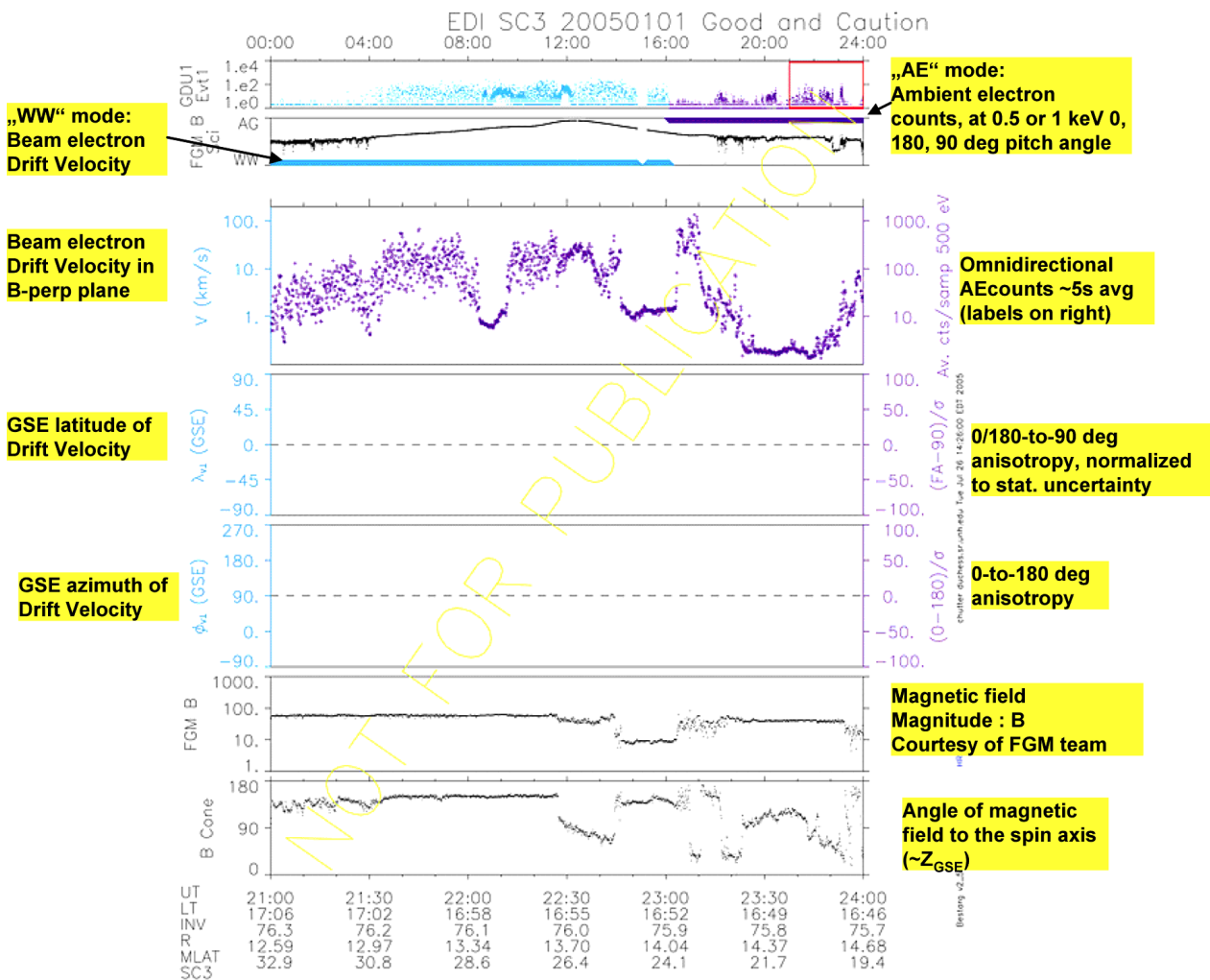
Figure 6 Example of EDI SUMMPLOT for 2005-01-01

The quick-look plots show the data measured by EDI for one reference spacecraft, mostly Cluster 3, for three hourly intervals using different colours for the 2 operation modes (blue for "WW" and purple for "AE". The top two panels show data for 24 hours: the first one is for ambient electron counts where the red square marks the three-hour interval shown in detail below in panels 3-7, and the second one is for the FGM magnetic field magnitude. This interval contains data only from the ambient mode for which the labels are shown on the right while the labels on the left are for the electric field mode. The two anisotropy panels are empty since this example contains only 90° pitch angle observations.

6 Recommendations

6.1 Electric field:

- Use SPIN data for electron drift/electric field if spin resolution is enough, since the bad quality data are removed.

- If a higher time resolution is needed, use the MP dataset. As it also contains the "bad" data, use the "Status" parameter to filter out the bad-quality data.

6.2 Ambient Electron Data:

- Use corrected ambient electron counts mainly for boundary recognition.
- Any further usage requires an inter-detector correction and even a relative calibration to PEACE data if electron fluxes are needed. The correction procedure is described in the EDI Cross-Calibration Report [6].
- In electric field mode one can use "***Background electron counts (in WW-mode)" for*** boundary crossing survey.

Appendix A

The EDI datasets stored in the CAA are listed in Table A1. The red colour is used to highlight the suffix that is often used as an acronym of the dataset. The blue colour is used to indicate the datasets that are given in text format, that is, these datasets are not available in CEF.

Table A1. Dataset ID and title for the EDI data products in the CAA. (n) is a placeholder for the spacecraft number: 1, 2, and 3 for EDI since EDI was switched off on Cluster 4.

Dataset ID	Dataset title in the CAA
Science datasets	
C(n)_CP_EDI_**MP**	Electron Drift Velocity and Electric Field (GSE), best resolution
C(n)_CP_EDI_**SPIN**	Electron Drift Velocity and Electric Field (GSE), spin resolution
C(n)_CP_EDI_**AEDC**	Corrected ambient electron counts
Ancillary datasets	
C(n)_CP_EDI_ **AE**	Ambient electron counts
C(n)_CQ_EDI_ **CLIST**	Caveats
C(n)_CE_EDI_ **QSTAT**_TXT	Quality Statistics for Electron Drift Velocity measurements
C(n)_CP_EDI_ **CRF**	Code Repetition Frequency
C(n)_CP_EDI_ **QZC**	Background electron counts (in WW-mode)
C(n)_CP_EDI_ **EGD**	Electron Gyrotime
C(n)_CG_EDI_ **SUMMPLOT**	EDI Summary Plot
C(n)_CE_EDI_ **AEC**_TXT	Ambient electron correction files
C(n)_ **PP** _EDI	Preliminary Electron Drift Velocity (GSE), spin resolution
C(n)_ **SP** _EDI	Preliminary Electron Drift Velocity (GSE), 1 minute resolution

The following EDI datasets stored in the CAA are available only through the command-line interface (see [8]) as they are only made available for reference (and for expert users). These products are mostly in CDF or internal raw data (BIN) format. They are further described in the ICD. The suffix in red is an acronym often used for the respective dataset. The letters in blue show the format of the files.

Table A2. Dataset ID for the EDI products that are available only through command line interface

Dataset ID
C#_CE_EDI_**MP**_CDF
C#_CE_EDI_**PP**_ CDF
C#_CE_EDI_**SP**_ CDF
C#_CE_EDI_**PPPLUS**_ CDF
C#_CE_EDI_**AE**_ CDF
C#_CE_EDI_ **MSF**_BIN

Note that in previous versions of the ICD, User Guide or in papers on EDI CAA data products the used acronyms differ slightly from the current ones that were taken from the group of letters appearing in the file and parameter names (e.g. MP and AE had an additional "D" or PPP appeared as PPplus, SUMMPLOT as 3hSPlot). Table A3 gives a summary of the acronyms, format, origin of the acronyms, content(C), quality(Q), time resolution(R) and dataset processing level.

Table A3. Summary of EDI products in the CAA

Acronym	Format	Name, content (C), quality (Q), time resolution (R)	Dataset Processing level
PP **SPIN**	CEF CDF	**P**rime **P**arameter / **SPIN**-Resolution Parameter C: Electric Field, Drift Velocity, status, errors Q: winners, good/caution R: spin (~4s)	calibrated
SP **Only Cluster 3**	CEF CDF	**S**ummary **P**arameter C: Electric Field, Drift Velocity, status, errors Q: winners, good/caution R: 1 min	calibrated
PPPlus	CDF	**P**rime **P**arameter **Plus** C: Electric Field, Drift Velocity, status, errors, drift step Q: winners + losers good/caution/bad R: spin (~4s)	calibrated
MP	CDF CEF	**M**erged **P**arameter **D**ata C: Electric Field, Drift Velocity, status and errors R: 1-4 s Q: winners, good/caution/bad	calibrated
AE **AEDC**	CDF CEF	**A**mbient **E**lectron & Corrected **A**mbient **E**lectron **D**ata C: Ambient electron counts at three pitch angles (0°/180° and/or 90°), electron energy, detector look direction R: full	uncalibrated
SUMMPLOT **Mostly Cluster 3**	PNG	**3-h**ourly **S**urvey **PLOT**s C: MPD, AED and CLIST parameters for one spacecraft	uncalibrated
EGD	CEF	**E**lectron **G**yrotime **D**ata C: Electron time-of-flight, error and GDU-flag R: full	auxiliary
QSTAT	ASCII	**Q**uality **STAT**istics C: EDI detection efficiency (beam tracking performance) R: 10 min	auxiliary
CLIST	CEF	**C**aveat **L**ist C: Time intervals of EDI operation modes (WW/AE)	auxiliary
AEC	ASCII	**AE C**orrection **f**iles Used to correct raw, ambient electron counts for theta/phi	auxiliary
CRF	CEF	**C**ode **R**epetition **F**requency C: Code repetition frequency, beam current index, R: telemetry (~5.12s)	auxiliary
QZC	CEF	**Q**uality **Z**ero **C**ounts C: raw electron counts (for PA=90°, E=0.5/1 keV), detector look direction R: full	auxiliary
MSF	Binary	**M**erged **S**cience **F**iles C: Merged HK+NM+BM	raw

Appendix B

The electron-drift technique is based on the injection of weak beams of electrons, in a direction perpendicular to the ambient magnetic field, and their detection after one or more gyrations. In a uniform magnetic field with no other forces acting, an electron beam fired in any direction perpendicular to the ambient magnetic field, **B**, will execute a circular gyro orbit and return to its starting point. In the presence of a drift velocity V_d, induced by an electric field E or a magnetic-field gradient ∇B **,** the circular electron orbits are distorted into cycloids. Their shape depends on whether the beam is injected with a component parallel or anti-parallel to the drift velocity. This perturbation can be measured in two different ways in order to determine the magnitude and direction of the electron drift velocity. The first method, triangulation, uses the fact that the perturbed trajectory of an electron beam, fired perpendicular to the ambient magnetic field, returns to the spacecraft after one or more gyro orbits only when fired in unique directions. The second method measures the times-of-flight for the electron beams to return to the spacecraft, which in the presence of a drift, differ from the gyroperiod by amounts that are proportional to $\pm\, V_d$.

Triangulation (TRI) method

For each gun only one orbit-solution exists that connects it with the detector on the opposite side of the spacecraft. Knowledge of the positions of the guns, and of the firing directions that cause the beams to hit their detectors, uniquely determines the drift velocity. This is the basis of the triangulation technique.

Through triangulation, one directly determines the 'drift-step' vector **d**, which is the displacement of the electrons after a gyrotime T_g:

$$\mathbf{d} = \mathbf{V}_d\, T_g. \tag{1}$$

A measurement of the drift step, together with the knowledge of the gyroperiod, is thus sufficient to determine the drift velocity.

The EDI triangulation technique is illustrated conceptually in **Figure B1**(a), which is drawn in the plane perpendicular to **B** (the "$B_\perp$ plane"). There are two electron guns, with a virtual detector (Det) located halfway in between. Red and blue lines represent the electron beams. The electron gyroradius is very large (> 1 km) compared to the scale of the figure (~1 m), so the gyro-trajectories of the beams appear as straight lines. The magnitude and orientation of the drift step, **d**, is determined by the ambient fields, as described above. We have drawn **d** with its head positioned at the detector. By definition of the drift step, any 90° pitch-angle electron passing through the tail end of **d** will be displaced by the drift velocity and will hit the detector exactly one gyroperiod later. The location in the B - plane, from which electrons reach the detector after one gyration, can be viewed as the 'target' for the electron beams. Electrons hitting the target after one gyration are called single-runners, after two gyrations double-runners and so on.

$$\vec{d} = (\vec{V}_{drift})(T_{gyro})$$

Figure B1 (a) Principle of the triangulation method

(b) Example of TRI analysis of 4 s of data [3]. Gun1 and Gun2 locations are indicated by asterisks and triangles, respectively, the emitted beams are shown as dashed and solid lines, respectively. The spacecraft appears as shaded circle.

An example of triangulation analysis is given in **Figure B1** (b). The figure shows gun locations and firing directions for a 4 s (i.e. one spin) interval during which beams happened to be aimed at the single- and double-runner targets. Gun1 and Gun2 locations are indicated by asterisks and triangles, respectively, the beams emanating from there guns are shown as dashed and solid lines, respectively. The (red) vector from the solid black circle to the centre of the spacecraft is the drift step (1.5 m in this case); it has been obtained from the best fit to all the beams in this interval. The solid circles are placed at integer multiples of the drift step from the centre of the spacecraft. The magenta-coloured beams are identified as double-runners. Yellow and Green dots mark the locations of triple- and quadra-runners but none exist in this case.

Note that the construction of the drift step from the firing directions of the beams is for a virtual detector location at the centre of the spacecraft. Thus, the spacecraft is drawn at twice its actual dimensions, as explained in [3]. The red vector from the solid black circle to the centre of the spacecraft is the drift step, determined, in the way described above, as the best fit to all the beams in the chosen interval. The figure emphasizes the importance of the correct identification of the multi-runners, in this case double-runners only. The example is for a less than perfect focus to illustrate the power of the statistical approach of this analysis technique. The analysis fails if the drift step and/or the magnetic field significantly vary within the chosen time interval. We can identify such cases by the variance in the magnetic field, by the quality of the fit (as measured by its reduced_chi_sq), and by the angle or magnitude errors in the computed drift step. If those quantities exceed certain limits, no output is generated. The EDI analysis software (EDI_PISO) uses for triangulation a threshold 50 for the reduced_chi_sq.

Time-of-Flight (TOF) method

Figure B2 shows two cycloid-shaped trajectories of the electrons that connect the guns with the detectors from the opposite side are drawn for very high drift velocity (Vd=1000 km/s and unrealistically large magnetic field (12000 nT) implying an equally unrealistic E field of 12 V/m, but a reasonable drift d=3m in order to make visible the differences between the trajectories. The different lengths of the two orbits are evident and this means they have also different travel times.
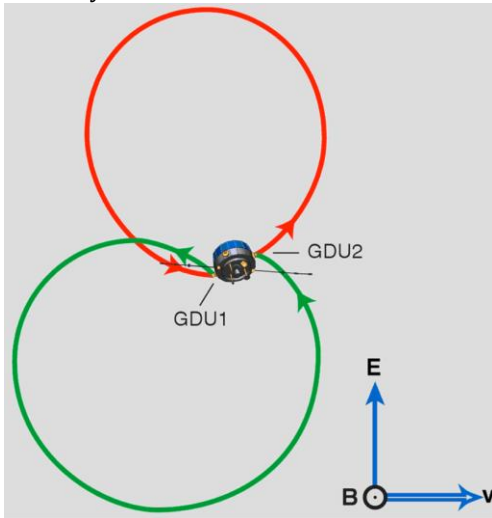
Figure B2 shows the principle of EDI operation. It is taken from [2].

The electrons emitted with their velocity directed with a component parallel to Vd , i.e. away from the target, have a time of flight that is shorter than Tg, while the electrons emitted towards the target have a time of flight that is longer than Tg:

$$T1,2 = Tg (1 \pm Vd/Ve)$$
$$(2)$$

where V_e is the electron velocity. From this equation it follows immediately that the difference between the two times-of-flight provides a measure of the drift velocity, V_d :

$$\Delta T = T1 - T2 = 2 (Vd / Ve) Tg = 2 (d / Ve) \tag{3}$$

while their sum is twice the gyro time: $T1 + T2 = 2 Tg$. Note that $Tg = 2 \pi me / (e B)$; this means that the time-of-flight measurements allow B being determined as well. Drift velocities encountered on a Cluster orbit typically are in the range of 1-1000 km/s, while the velocity of 1 keV electrons is ~20 000 km/s. This implies that ΔT is only a small fraction of Tg, i.e., the drift introduces only a small variation in the two orbits and the associated times-of-flight. In order to measure the electron times-of-flight, as well as to distinguish beam electrons from the background of ambient electrons, the electron beams are amplitude-modulated with a pseudo-noise (PN) code. The code repetition frequency (in the kHz range) is interfering with the wave instruments.

Estimate of errors on EDI electric field

This section gives an example of error estimation for the electric field. It is given to show the difficulties related to such a task and to explain why these errors are not given in the dataset.

The EDI CAA electric field datasets (PP, MP and PPPlus) contain two error estimates stored in the "Status" variable (see Chapter 4): Status(5) is the fractional error on the drift step magnitude, and Status(6) is the angular error of the drift step vector, in degrees. Both are computed and reported in the satellite frame of reference. These errors are reported for both the triangulation and time-of-flight methods.

For triangulation, the drift step magnitude error is determined from the maximum radial extent of the 90% confidence level iso-contour of the 2-D penalty function surface surrounding the localized minimum which has been chosen as the "best" (in a statistical sense) answer for the drift step target. The angular error is defined as the maximum angular extent of this iso-contour.

For the time-of-flight method, the errors are computed differently. The electron beam firing directions are to a high degree all co-linear in this regime and triangulation isn't possible. The firing directions are split into two distributions, those pointing away from the spacecraft in one general direction, and those pointing away from the spacecraft in the opposite direction. The group with the larger values of times-of-flight are assigned the "towards" group, and the other is assigned the "away" group. The "towards" group, with the larger times-of-flight, are known to be firing parallel to the drift step vector, while the "away" group fires anti-parallel to this direction. The drift step vector direction is thus computed as the average direction of the "towards" group. The standard deviation of this average is reported as the drift step angular error. The "towards" times-of-flight are averaged, as well as the "away" times-of-flight. The difference between the time-of-flight averages, i.e., "towards" average minus "away" average, is labelled "delta_tof". The drift step magnitude is computed as delta_tof times the beam velocity divided by 2. The error on the drift step magnitude is computed using the "Student's t-test", which measures the significance of a difference of means [e.g., Numerical Recipes by Press et al.]. The error is reported at the 90% confidence level.

Propagation of the drift step error information collected in the spacecraft frame, to the 3-component electric field vector in an inertial frame (say, GSE) involves several steps, and must account for additional sources of error in parameters such as the magnetic field, the spacecraft velocity and spacecraft attitude. Errors are not routinely reported on these additional parameters, which makes full error propagation difficult.
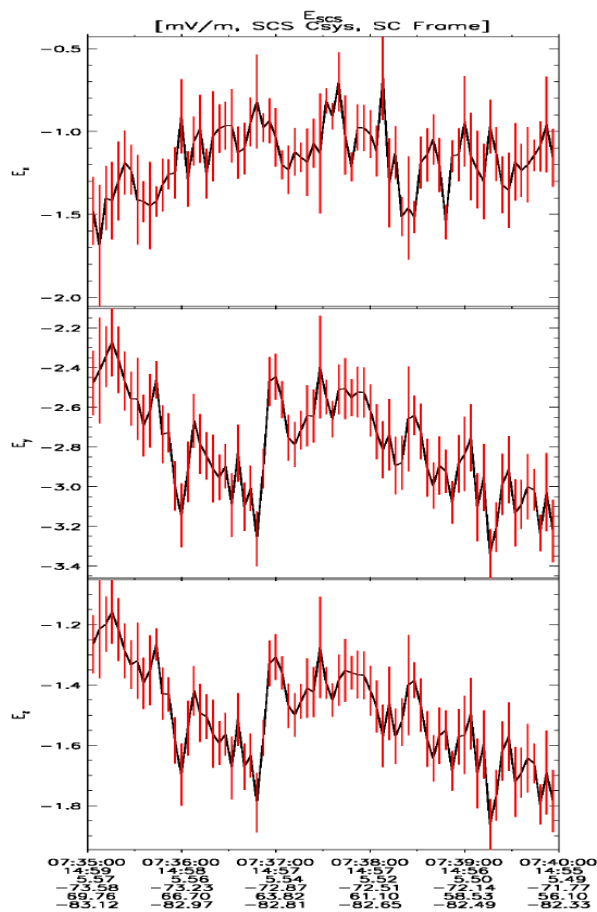
E_{scs}
[mV/m, SCS Csys, SC Frame]

Figure B3 Example of computed errors on **E** in the SCS coordinate system in the spacecraft frame. The calculation was done from 07:35-07:40 UT on 16-Jul-2001 on Cluster 3. From top to bottom are Ex, Ey and Ez. The data is plotted in black, and the computed errors overplotted in red. In the Ex panel, you have Ex ~ -1 +/- 0.2 mV/m, or, a 20% error. In the Ey panel, you have Ey ~ -2.8 +/- 0.2 mV/m, or a 7% error. And in the Ez panel, you have Ez ~ -1.5 +/- 0.1, or a 7% error. **These errors are highly specific to this particular case and cannot be used to generalize error estimates for the entire dataset. A careful, detailed, case-by-case error analysis must be performed to properly estimate errors for other time intervals.**

We have, however, for selected cases, such as for Figure B3, ignored these additional errors, and computed errors on all three components of the electric field in spacecraft coordinates (SCS) and in the spacecraft frame. The steps involved for the propagation include:

1. Extract the EDI drift velocity, **V**, and drift step errors from the CAA EDI dataset
2. Transform **V** into the spacecraft frame
3. Extract the FGM magnetic field, **B**, from the CAA FGM dataset
4. Compute the electric field, **E**, using the **V** and **B**
5. Rotate **V**, **E** and **B** into spacecraft coordinates (SCS)
6. Rotate **V** and **E** into the "**B**-perp plane" (this is called the BPP coordinates) which are the coordinates used for EDI analysis
7. Compute the gyro-time using **B**
8. Compute the drift step vector, **d**, in BPP coordinates using **V** and the gyro-time
9. Define the "target" vector as **d** flipped by 180 degrees
10. Define the "error swath" area around the target vector head using the drift step magnitude and angular errors extracted from the EDI dataset
11. Rotate and scale the error swath to represent the error on the drift velocity vector head (the fractional error is preserved)
12. Rotate and scale the error swath to represent the error on the electric field vector head (the fractional error is preserved)
13. Rotate **E** and its error swath back to SCS coordinates
14. Define errors for each component of **E** in SCS as the maximum extent of the projected error swath for that component divided by 2

Appendix C - magnetic gradient effects

The electric field and gradients in the magnetic field both contribute to the drift velocity. As the ∇B drift depends on the electron energy, while the electric field drift does not, the two drifts could in principle be separated by employing two different electron energies. Since the ∇B drift is usually small compared with the electric field drift, and the energy switching complicates beam tracking, energy switching has not been a standard operating mode. It has been exercised at the beginning of the mission, but the obtained results showed that the ∇B drift effect was below the errors associated with the drift step measurement. Under the assumption that the ∇B -drift can be ignored, the electric field can be computed according to:

$$E \simeq -V_d \times B$$

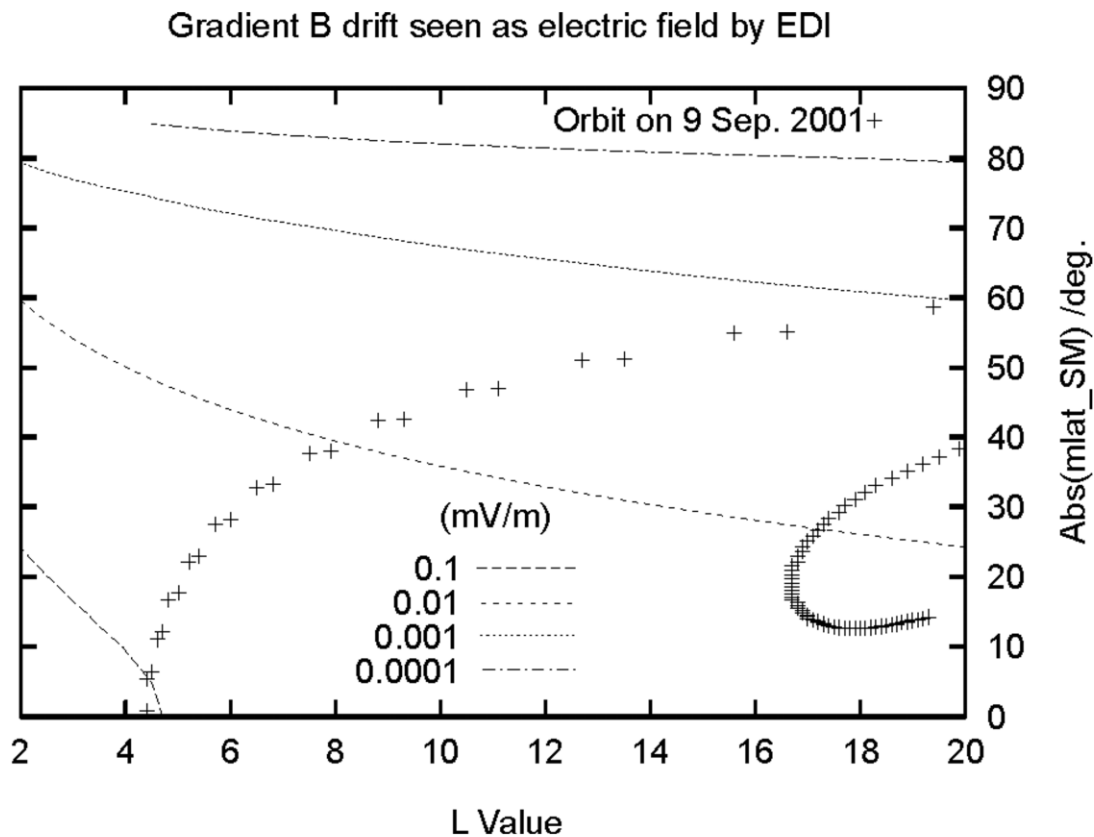Figure C1 exemplifies the ∇B drift for 1 keV electrons for a Cluster orbit on 2001-09-09.

Figure C1. Gradient B drift seen as electric field by EDI (beam energy=1 keV, dipole magnetic field, mapped to equatorial value) [credit: Hiroshi Matsui]

The orbit and the isoclines for different orders of magnitude of gradient B drift are projected on the L-value, absolute magnetic latitude plane and have been computed using a dipole field model. The highest value is 0.1 mV/m and is reached by L-values around 4 where the electric field of interest is larger than 2 mV/m. In conclusion in most of the cases when EDI has measurements the grad **B** effect is negligible.

Appendix D – "multi-runners"

It is often assumed that the beam electrons are detected after a single gyration. Electrons that have gyrated N times will have a drift step and ΔT that is N times larger. As we will see, electrons having gyrated several times ('multi-runners') are indeed observed. We will refer to N as the multi-runner order. This phenomenon can be seen as an aliasing effect and specific software has been developed to take care of it. The software is part of the time-of-flight analysis and performs the 'runner order' determination for each reported hit in telemetry. This determination is made regardless of whether triangulation analysis or time-of-flight analysis is chosen. For the time-of-flight analysis this determination is mandatory, as the times-of-flight of multi-runners (order >=2) need to be turned into corresponding single-runner times-of-flight before performing averaging. For the triangulation analysis, using the results from the runner order determination is preferable to letting the chi-square fitting routine figure out the runner orders, as this reduces the number of degrees of freedom in the fit. Under certain conditions (magnetic field strength vs. chosen correlator code period) the determination of runner orders cannot be made unambiguously. In that case the possible runner orders are returned and the chi-square fitting routine needs decide on the best runner order.

Appendix E – Time-aliasing effects

One kind of aliasing is based on the period of the modulation code and the time width that is covered by the 15 correlator counters. The on-board software takes the magnetic field values received from FGM and turns them into a gyro time. The chain of 15 correlator counters is initially placed such that a return beam that travelled for exactly one gyro time before returning to the detector will appear as a peak in the centre of the correlator chain (called "channel 7"). Offsets in the magnetic field from FGM and non-zero electric fields both cause the peak to deviate from the centre channel. If this combined effect causes the deviation from channel 7 to be more than 7.5 code chip widths, the peak will appear at the other end of the correlator counter chain and thus be aliased.

The top panel of Figure E1 shows the maximum electric field that can be measured without aliasing when using short code as a function of the magnetic field magnitude for an assumed magnetic field offset of 0.3 nT. The black points are for electron beam energy of 1 keV, the red point for 500 eV. The jumps are caused by factor-of-two switching of the modulation code chip length at certain magnetic field magnitudes. The bottom panel shows the drift velocities associated with these electric field limits. This illustrates that for the chosen operational parameters (code period as a function of B magnitude, number of correlator counters) this kind of aliasing is not a problem, as the minimum drift velocity at which aliasing occurs is around 500 km/s. Such high drift velocities cannot be measured with EDI on Cluster, because in regions where they occur the magnetic field is too low and too variable for EDI to work successfully.
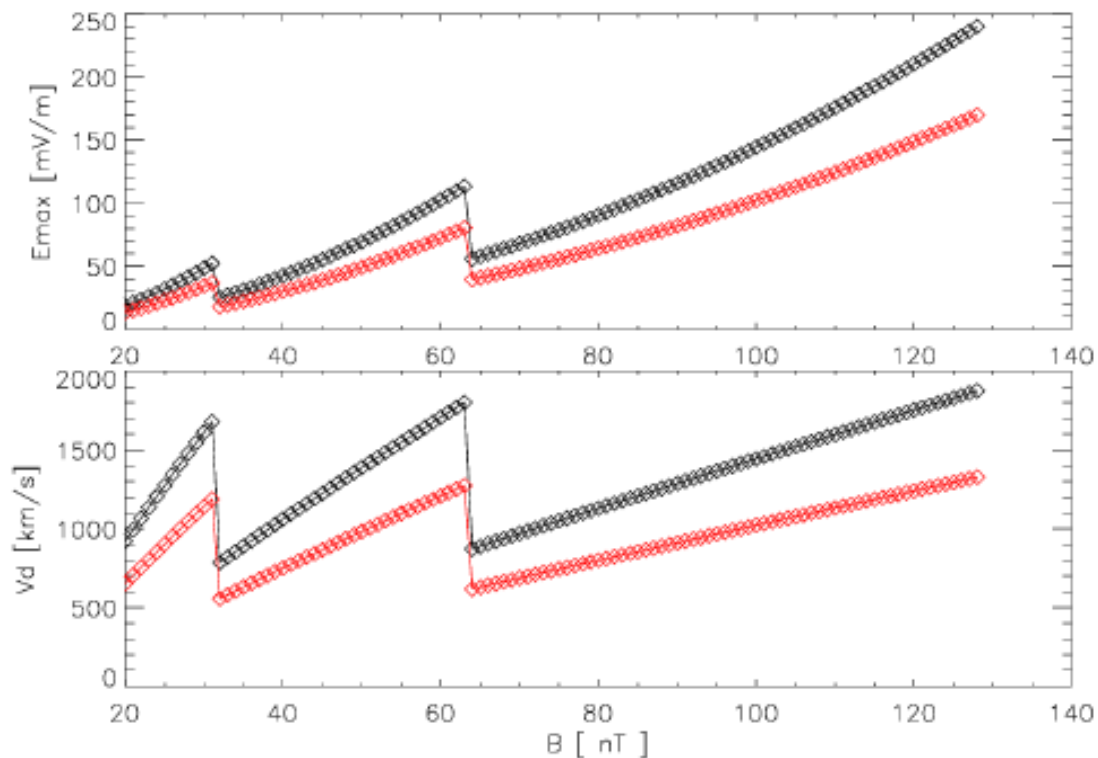

Figure E1 Maximum E-field and maximum drift velocity without aliasing for short code, magnetic field offset 3 nT, electron energy = 1 keV (black curves) and 0.5 keV (red curves).

Appendix F - Data coverage and variability

In order to represent variability of the data we use the total variance, which is commonly used to represent statistical errors of EDI measurements (e.g. Forster et al., 2007 [9]; Haaland et al., 2008 [10]). The total variance is expressed as follows:

$$\sigma_{tot}^2 = \frac{\langle |V|^2 \rangle - |\langle V \rangle|^2}{\langle |V|^2 \rangle},$$

V is measured drift velocity, and $\langle \ldots \rangle$ denotes an average in the chosen period. The total variance is normalized and describes the overall changes of the vector (both in magnitude and direction). Zero value of the total variance indicates the steady convection in chosen period, while the values close to unity indicate high variability of the convection. In order to determine the total variance, we have chosen the time window of 10 minutes. For each 10-minute window, the total variance is calculated, and assigned to the central time of the window. Two examples of this process are shown in the Figure 1 (variable and steady case). Yellow areas in the figure 1 represent the 10-minute window added for calculation of total variances. In first area velocities are rapidly changing and the calculated variance is close to one ($\sigma_{tot}^2 = 0.9056$). In second area the velocities are relatively stable, and the variance is close to zero ($\sigma_{tot}^2 = 0.14403$). For better statistical representation, at least 5 minutes of data were required in each of 10-minute window.
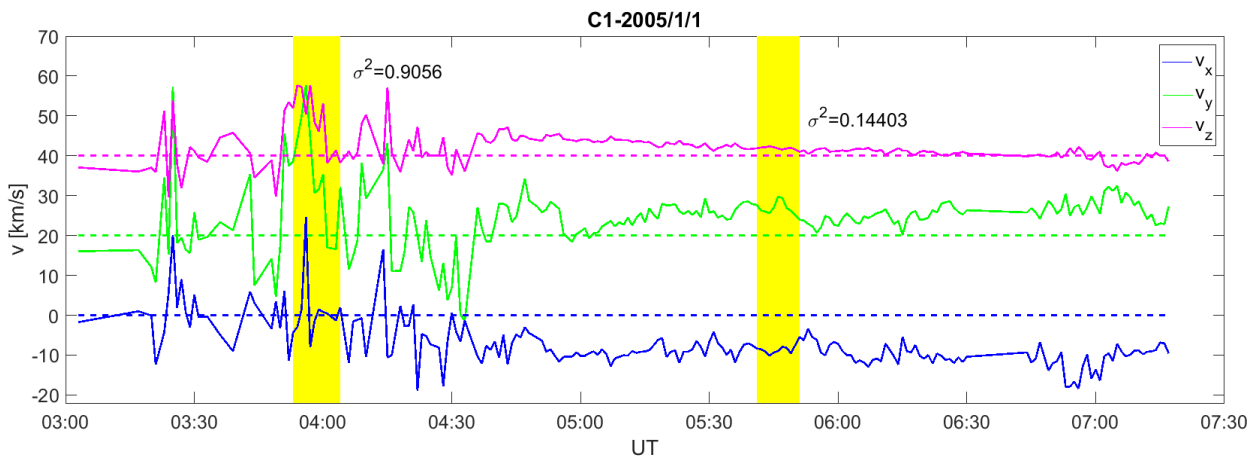

Figure 1: Examples of total variances. The solid lines show three different GSE velocity components measured with EDI onboard Cluster 1 on 1st of January 2005. The offset of 20 km/s was set between the components for a better comparison. The zero levels of each velocity components are represented with dashed lines. Yellow areas are 10-minute windows used to calculated total variance. The calculated total variances for each area are listed next to them.

To show the spatial variability, we have divided the tree standard GSM reference planes into $1x1R_E$ bins. The total variance in each bin is determined as the median of all total variances projected into that bin. The minimum number of required data points in each bin was set to 3. The results of this process are shown in Figure 2. As expected the EDI data are stable in the polar regions, and variable near the plasma sheet. All areas near magnetosphere boundary are variable because of the interaction with magnetosheath and the solar wind. Dawn-dusk asymmetry in variability can also be seen. The revolution of the Earth around the Sun causes the aberration of the magnetosphere, and tail curve of 4° towards positive GSE-y direction. Interesting thing is the stability of the EDI data near the Earth. This stability occurs because in this regions corotation electric field is dominant. (Matsui et. al., 2003; 2004).

Data used in Figure 2 have "good" and "caution" quality flags in the Cluster database.

Figure 3 shows the total variance distribution of Cluster data containing data flagged as "bad". These have higher total variability and should be used with care. One can clearly see that data with "bad" quality tags have high total variances and thus are very variable.
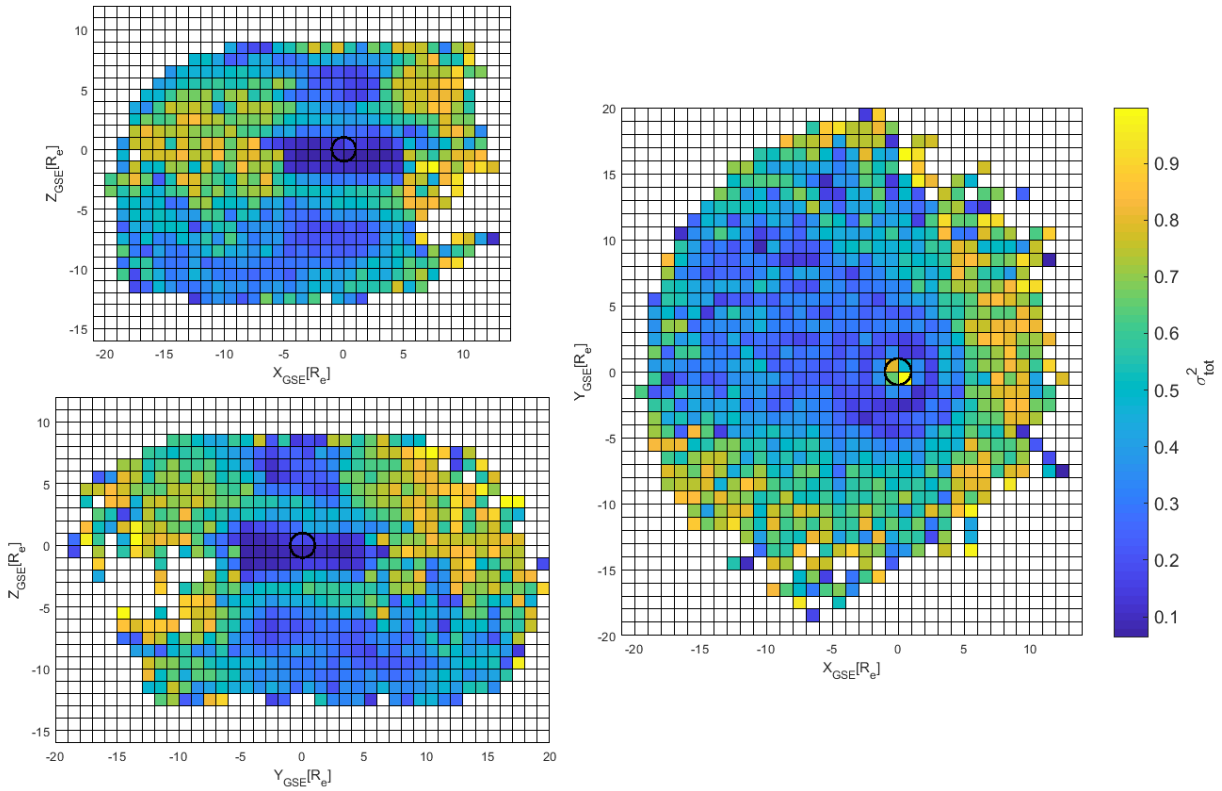
![esa logo]

Doc. No.	CAA-EST-UG-EDI
Issue:	4.2
Date:	2023-10-30

Project: Cluster Active Archive

Page: 28 of 30

Figure 2: The spatial distribution of the total variance of data with ''good'' and ''caution'' quality tags. The data are represented in three standard GSM reference planes. Each bin represents the projection of data on given reference plane.
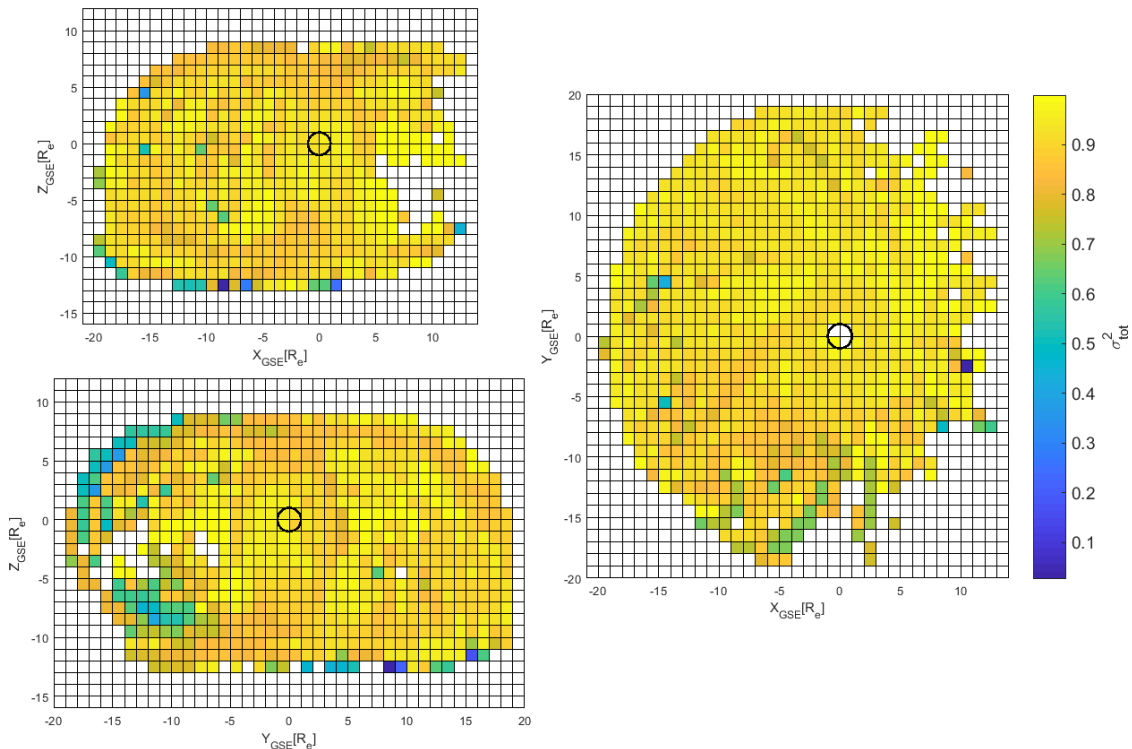

Figure 3: Total variance distribution of data with ''bad'' quality tag. The data are represented in three standard GSM reference planes. Each bin represents projection of data on given reference plane.

Doc. No.   CAA-EST-UG-EDI
Issue: 4.2
Date: 2023-10-30

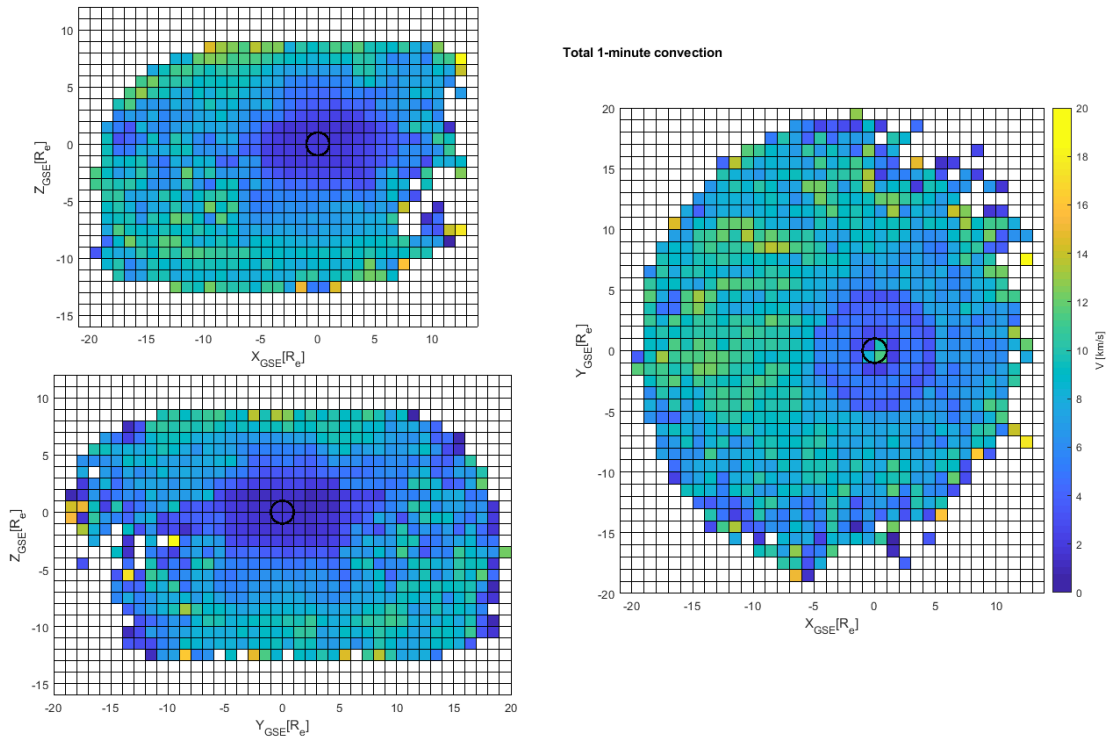Project: Cluster Active Archive   Page: 29 of 30

Figure 4: Absolute values of drift velocities averaged in one minute. The data are represented in three standard GSM reference planes. Each bin represents projection of data on given reference plane.
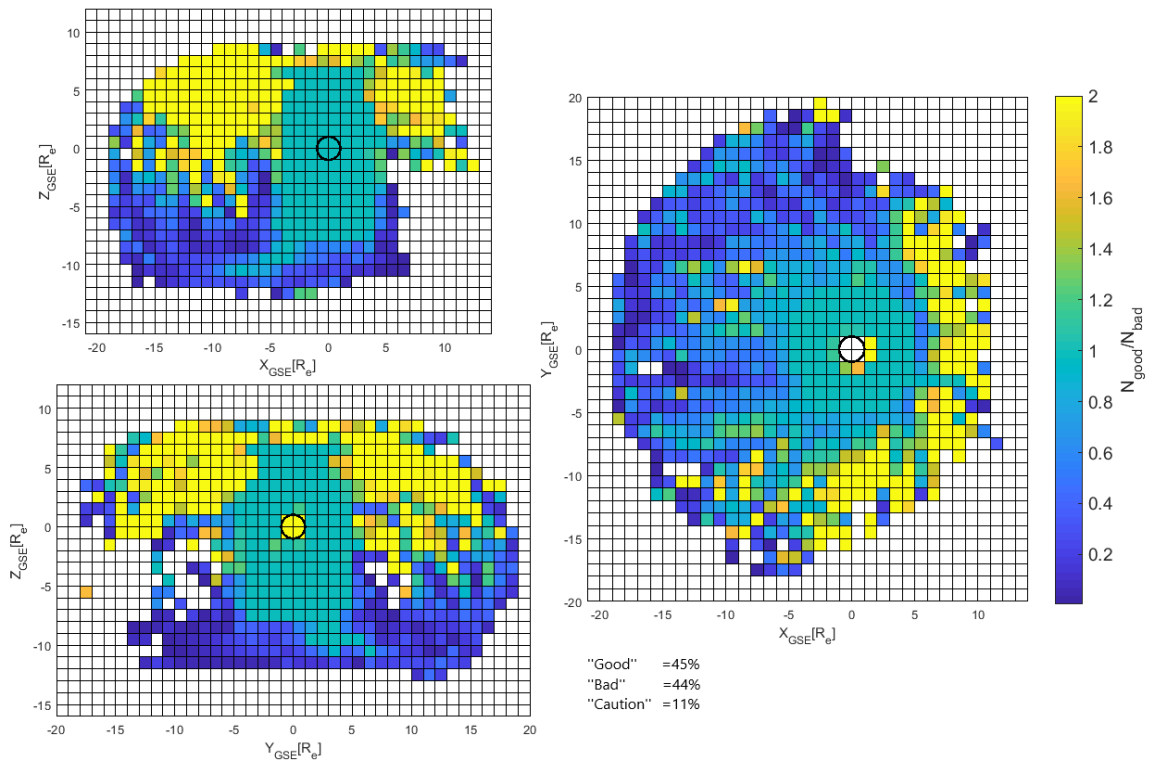

Figure 5: The ratio of "good" and "bad" data. The data in these plots are derived from years 2002-2009. In the right bottom of the figure are the percentages of data with each quality tag. The data are represented in three standard GSM reference planes. Each bin represents the projection of data on given reference plane.

Doc. No.   CAA-EST-UG-EDI
Issue: 4.2
Date: 2023-10-30

Project: Cluster Active Archive   Page: 30 of 30

Figure 4 shows 1minute averages of the magnitude of the velocity. Near Earth, at *5 Re* distance, typical velocities are less than *2 - 3 km/s*, and dominated by co-rotation. In northern hemisphere the velocities are in range *6-8 km/s,* and velocity increases as we move further from the Earth. This is caused by the convecting field lines that have one end "attached" to Earth and the other is "free" as explained by Dungey cycle [Dungey, 1964]. By moving away from Earth, the convection increases accordingly. In the southern hemisphere the drift velocities are slightly higher – typically, *8-10 km/s.* A possible explanation for this north-south asymmetry may be differences in the lobe magnetic field.

Figure 5 shows the distribution of ratio between ''good'' and ''bad'' data. If the ratio is higher than *1* then the region is dominated by data which is flagged as ''good'' in the Cluster data base. Accordingly, if the ratio is lesser than *1,* the region is dominated by ''bad'' data. The distribution ratio is nearly the same around the Earth and in the polar cup regions. Interesting thing is the north-south asymmetries in ratio. The northern lobe is dominated with ''good'' data, while in southern lobe dominate ''bad'' data. Here we offer possible explanation for such behaviour: the southern lobe has on average a weaker magnetic field and is more influenced by the external changes, than the northern lobe. One of the assumptions for good EDI measurements is that the magnetic field is relatively stable.